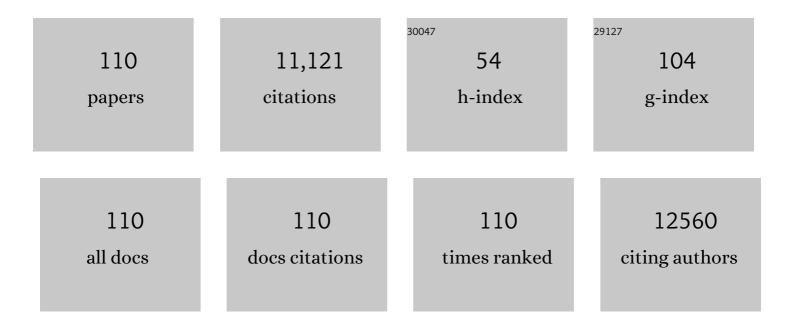
List of Publications by Year in descending order

Source: https://exaly.com/author-pdf/4775088/publications.pdf Version: 2024-02-01



#	Article	IF	CITATIONS
1	Electrospun Semiconductorâ€Based Nanoâ€Heterostructures for Photocatalytic Energy Conversion and Environmental Remediation: Opportunities and Challenges. Energy and Environmental Materials, 2023, 6, .	7.3	37
2	Interfacial electronic modulation of CoP-CoO p-p type heterojunction for enhancing oxygen evolution reaction. Journal of Colloid and Interface Science, 2022, 607, 1343-1352.	5.0	39
3	Electrostatic self-assembly to form unique LiNbO3/ZnS core-shell structure for photocatalytic nitrate reduction enhancement. Journal of Colloid and Interface Science, 2022, 607, 1323-1332.	5.0	17
4	One-dimensional CoP/MnO hollow nanostructures with enhanced oxygen evolution reaction activity. Journal of Colloid and Interface Science, 2022, 610, 663-670.	5.0	15
5	N-doping TiO2 hollow microspheres with abundant oxygen vacancies for highly photocatalytic nitrogen fixation. Journal of Colloid and Interface Science, 2022, 609, 341-352.	5.0	59
6	3D interconnected porous carbon derived from spontaneous merging of the nano-sized ZIF-8 polyhedrons for high-mass-loading supercapacitor electrodes. Journal of Materials Chemistry A, 2022, 10, 2027-2034.	5.2	23
7	Trimetallic CoNiFe-layered double hydroxides: Electronic coupling effect and oxygen vacancy for boosting water splitting. Journal of Power Sources, 2022, 524, 231068.	4.0	28
8	Activation of peroxymonosulfate by α-MnO2 for Orange â removal in water. Environmental Research, 2022, 210, 112919.	3.7	19
9	Manipulation of Mottâ^'Schottky Ni/CeO ₂ Heterojunctions into Nâ€Đoped Carbon Nanofibers for Highâ€Efficiency Electrochemical Water Splitting. Small, 2022, 18, e2106592.	5.2	73
10	Photothermal-effect-promoted interfacial OH ^{â^'} filling and the conversion of carrier type in (Co _{1â^'<i>x</i>} Ni _{<i>x</i>}) ₃ C during water oxidation. Journal of Materials Chemistry A, 2022, 10, 8258-8267.	5.2	6
11	One-dimensional Ni2P/Mn2O3 nanostructures with enhanced oxygen evolution reaction activity. Journal of Colloid and Interface Science, 2022, 623, 196-204.	5.0	11
12	Electrostatic self-assembled layered polymers form supramolecular heterojunction catalyst for photocatalytic reduction of high-stability nitrate in water. Journal of Colloid and Interface Science, 2022, 622, 828-839.	5.0	7
13	Construction of hierarchical ZnIn2S4@PCN-224 heterojunction for boosting photocatalytic performance in hydrogen production and degradation of tetracycline hydrochloride. Applied Catalysis B: Environmental, 2021, 284, 119762.	10.8	193
14	One-dimensional zinc-manganate oxide hollow nanostructures with enhanced supercapacitor performance. Journal of Colloid and Interface Science, 2021, 585, 138-147.	5.0	21
15	Template-Free Synthesis of One-Dimensional g-C3N4 Chain Nanostructures for Efficient Photocatalytic Hydrogen Evolution. Frontiers in Chemistry, 2021, 9, 652762.	1.8	5
16	ZIF-8-derived carbon-modified g-C ₃ N ₄ heterostructure with enhanced photocatalytic activity for dye degradation and hydrogen production. Dalton Transactions, 2021, 50, 17618-17624.	1.6	15
17	Smart Design, Controllable Synthesis, and Functional Applications of Low-Dimensional Hetero-Structured Materials. Journal of Nanomaterials, 2021, 2021, 1-2.	1.5	0
18	NiMoO4 nanorods@hydrous NiMoO4 nanosheets core-shell structured arrays for pseudocapacitor application. Journal of Alloys and Compounds, 2020, 814, 152253.	2.8	23

#	Article	IF	CITATIONS
19	Build-in electric field induced step-scheme TiO2/W18O49 heterojunction for enhanced photocatalytic activity under visible-light irradiation. Ceramics International, 2020, 46, 23-30.	2.3	99
20	Bimetal Networked Nanosheets Co x Ni 3â^'x S 2 as An Efficient Electrocatalyst for Hydrogen Evolution. ChemCatChem, 2020, 12, 609-614.	1.8	13
21	Preparation of heterometallic CoNi-MOFs-modified BiVO4: a steady photoanode for improved performance in photoelectrochemical water splitting. Applied Catalysis B: Environmental, 2020, 266, 118513.	10.8	208
22	Asymmetric supercapacitors by integrating high content Na+/K+-inserted MnO2 nanosheets and layered Ti3C2Tx paper. Electrochimica Acta, 2020, 332, 135497.	2.6	32
23	Superior uniform carbon nanofibers@g-C3N4 core-shell nanostructures embedded by Au nanoparticles for high-efficiency photocatalyst. Journal of Hazardous Materials, 2020, 388, 121759.	6.5	24
24	Immobilization of Ni ₃ Co Nanoparticles into Nâ€Đoped Carbon Nanotube/Nanofiber Integrated Hierarchically Branched Architectures toward Efficient Overall Water Splitting. Advanced Science, 2020, 7, 1902371.	5.6	89
25	A High apacity Negative Electrode for Asymmetric Supercapacitors Based on a PMo ₁₂ Coordination Polymer with Novel Waterâ€Assisted Proton Channels. Small, 2020, 16, e2001626.	5.2	124
26	Facile loading of cobalt oxide on bismuth vanadate: Proved construction of p-n junction for efficient photoelectrochemical water oxidation. Journal of Colloid and Interface Science, 2020, 570, 89-98.	5.0	70
27	Efficient and Stable Ideal Bandgap Perovskite Solar Cell Achieved by a Small Amount of Tin Substituted Methylammonium Lead Iodide. Electronic Materials Letters, 2020, 16, 224-230.	1.0	20
28	CO ₂ photoreduction to CO/CH ₄ over Bi ₂ W _{0.5} Mo _{0.5} O ₆ solid solution nanotubes under visible light. RSC Advances, 2020, 10, 8821-8824.	1.7	19
29	The synergetic effect of carbon nanotubes and MoS2 as co-catalysts for enhancing the photocatalytic oxygen evolution of Ag3PO4. Ceramics International, 2019, 45, 21120-21126.	2.3	27
30	Built-in electric field induced CeO2/Ti3C2-MXene Schottky-junction for coupled photocatalytic tetracycline degradation and CO2 reduction. Ceramics International, 2019, 45, 24146-24153.	2.3	152
31	Immobilization of Fe3N nanoparticles within N-doped carbon nanosheet frameworks as a high-efficiency electrocatalyst for oxygen reduction reaction in Zn-air batteries. Carbon, 2019, 153, 364-371.	5.4	74
32	A MoS2-Co9S8-NC heterostructure as an efficient bifunctional electrocatalyst towards hydrogen and oxygen evolution reaction. Electrochimica Acta, 2019, 327, 134942.	2.6	37
33	Flexible Ti ₃ C ₂ T _x /PEDOT:PSS films with outstanding volumetric capacitance for asymmetric supercapacitors. Dalton Transactions, 2019, 48, 1747-1756.	1.6	119
34	AgBr/BiOBr Nano-Heterostructure-Decorated Polyacrylonitrile Nanofibers: A Recyclable High-Performance Photocatalyst for Dye Degradation under Visible-Light Irradiation. Polymers, 2019, 11, 1718.	2.0	36
35	Cobaltâ€Embedded Nâ€Doped Carbon Arrays Derived In Situ as Trifunctional Catalyst Toward Hydrogen and Oxygen Evolution, and Oxygen Reduction. ChemElectroChem, 2019, 6, 4522-4532.	1.7	17
36	The surface engineering of cobalt carbide spheres throughÂN, B co-doping achieved by room-temperature <i>in situ</i> anchoring effects for active and durable multifunctional electrocatalysts. Journal of Materials Chemistry A, 2019, 7, 14904-14915.	5.2	88

#	Article	IF	CITATIONS
37	Co(OH)F nanorods@K _x MnO ₂ nanosheet core–shell structured arrays for pseudocapacitor application. RSC Advances, 2019, 9, 36208-36212.	1.7	6
38	Asymmetric supercapacitors with excellent rate performance by integrating Co(OH)F nanorods and layered Ti ₃ C ₂ T _x paper. RSC Advances, 2019, 9, 30957-30963.	1.7	13
39	Annealing temperature dependent ZnCo2O4 nanosheet arrays supported on Ni foam for high-performance asymmetric supercapacitor. Journal of Alloys and Compounds, 2019, 773, 367-375.	2.8	35
40	Ultrathin AgPt alloy nanowires as a high-performance electrocatalyst for formic acid oxidation. Nano Research, 2018, 11, 499-510.	5.8	86
41	Ag-Nanoparticle-Decorated 2D Titanium Carbide (MXene) with Superior Electrochemical Performance for Supercapacitors. ACS Sustainable Chemistry and Engineering, 2018, 6, 7442-7450.	3.2	120
42	A Solid‣tate Fibriform Supercapacitor Boosted by Host–Guest Hybridization between the Carbon Nanotube Scaffold and MXene Nanosheets. Small, 2018, 14, e1801203.	5.2	158
43	Free-standing Ti ₃ C ₂ T _x electrode with ultrahigh volumetric capacitance. RSC Advances, 2017, 7, 11998-12005.	1.7	98
44	Three-dimensional porous ZnCo2O4 sheet array coated with Ni(OH)2 for high-performance asymmetric supercapacitor. Journal of Colloid and Interface Science, 2017, 497, 50-56.	5.0	55
45	Facile synthesis of ZnCo2O4 micro-flowers and micro-sheets on Ni foam for pseudocapacitor electrodes. Journal of Alloys and Compounds, 2017, 702, 381-387.	2.8	31
46	A Nonmetal Plasmonic Zâ€Scheme Photocatalyst with UV―to NIRâ€Driven Photocatalytic Protons Reduction. Advanced Materials, 2017, 29, 1606688.	11.1	345
47	Graphitic Carbon Nitride Isotype Heterostructures with Enhanced Visible Photocatalytic Properties. Nano, 2017, 12, 1750042.	0.5	6
48	Performance evaluation of asymmetric supercapacitor based on Ti3C2Tx-paper. Journal of Alloys and Compounds, 2017, 729, 1165-1171.	2.8	26
49	New Ti 3 C 2 aerogel as promising negative electrode materials for asymmetric supercapacitors. Journal of Power Sources, 2017, 364, 234-241.	4.0	205
50	Construction of Hierarchical Ni(OH) ₂ @CoMoO ₄ Nanoflake Composite for High-Performance Supercapacitors. Nano, 2016, 11, 1650050.	0.5	9
51	Visible/near-IR-light-driven TNFePc/BiOCl organic–inorganic heterostructures with enhanced photocatalytic activity. Dalton Transactions, 2016, 45, 9497-9505.	1.6	47
52	A bismuth oxide nanosheet-coated electrospun carbon nanofiber film: a free-standing negative electrode for flexible asymmetric supercapacitors. Journal of Materials Chemistry A, 2016, 4, 16635-16644.	5.2	124
53	A Rapid Microwaveâ€Assisted Thermolysis Route to Highly Crystalline Carbon Nitrides for Efficient Hydrogen Generation. Angewandte Chemie, 2016, 128, 14913-14917.	1.6	234
54	A Rapid Microwaveâ€Assisted Thermolysis Route to Highly Crystalline Carbon Nitrides for Efficient Hydrogen Generation. Angewandte Chemie - International Edition, 2016, 55, 14693-14697.	7.2	335

#	Article	IF	CITATIONS
55	Crystalline NiCo2S4 nanotube array coated with amorphous NiCo S for supercapacitor electrodes. Journal of Colloid and Interface Science, 2016, 467, 140-147.	5.0	85
56	Generation of Oxygen Vacancy and OH Radicals: A Comparative Study of Bi ₂ WO ₆ and Bi ₂ WO _{6a^^<i>x</i>} Nanoplates. ChemCatChem, 2015, 7, 4076-4084.	1.8	117
57	One-dimensional Ag ₃ PO ₄ /TiO ₂ heterostructure with enhanced photocatalytic activity for the degradation of 4-nitrophenol. RSC Advances, 2015, 5, 29693-29697.	1.7	31
58	NiCo2S4/Ni(OH)2 core-shell heterostructured nanotube arrays on carbon-fabric as high-performance pseudocapacitor electrodes. Applied Surface Science, 2015, 349, 870-875.	3.1	47
59	Controllable synthesis of Ni3â^'xCoxS4nanotube arrays with different aspect ratios grown on carbon cloth for high-capacity supercapacitors. RSC Advances, 2015, 5, 48631-48637.	1.7	29
60	Silver-decorated orthophosphate@bismuth molybdate heterostructure: An efficient photocatalyst with two visible-light active components. Journal of Molecular Catalysis A, 2015, 400, 154-161.	4.8	13
61	Nanosize α-Bi ₂ O ₃ decorated Bi ₂ MoO ₆ via an alkali etching process for enhanced photocatalytic performance. RSC Advances, 2015, 5, 12346-12353.	1.7	48
62	Bismuth oxychloride/carbon nanofiber heterostructures for the degradation of 4-nitrophenol. CrystEngComm, 2015, 17, 7276-7282.	1.3	20
63	Direct Growth of Bismuth Oxyhalides Nanosheet Arrays on Carbon Cloth for Recycled Photocatalytic Degradation of Dye and 4-Nitrophenol. Nano, 2015, 10, 1550066.	0.5	4
64	NiMoO ₄ @Ni(OH) ₂ core/shell nanorods supported on Ni foam for high-performance supercapacitors. RSC Advances, 2015, 5, 69365-69370.	1.7	35
65	Effect of temperature on pseudocapacitance performance of carbon fiber@NiCo 2 O 4 @Ni(OH) 2 core–shell nanowire array composite electrodes. Applied Surface Science, 2015, 356, 167-172.	3.1	29
66	In situ ion exchange synthesis of the Bi4Ti3O12/Bi2S3 heterostructure with enhanced photocatalytic activity. Catalysis Communications, 2015, 60, 23-26.	1.6	36
67	Ultrathin hexagonal SnS2 nanosheets coupled with g-C3N4 nanosheets as 2D/2D heterojunction photocatalysts toward high photocatalytic activity. Applied Catalysis B: Environmental, 2015, 163, 298-305.	10.8	616
68	BiOCl nanosheet/Bi4Ti3O12 nanofiber heterostructures with enhanced photocatalytic activity. Catalysis Communications, 2015, 58, 122-126.	1.6	42
69	Piezoelectric nanogenerator based on a flexible carbon-fiber/ZnO–ZnSe bilayer structure wire. Applied Surface Science, 2014, 322, 95-100.	3.1	20
70	Enhanced photosensitization process induced by the p–n junction of Bi2O2CO3/BiOCl heterojunctions on the degradation of rhodamine B. Applied Surface Science, 2014, 303, 360-366.	3.1	142
71	Controllable synthesis and enhanced visible photocatalytic degradation performances of Bi2WO6–carbon nanofibers heteroarchitectures. Journal of Sol-Gel Science and Technology, 2014, 70, 149-158.	1.1	12
72	Electrospun Pt/TiO 2 hybrid nanofibers for visible-light-driven H 2 evolution. International Journal of Hydrogen Energy, 2014, 39, 19434-19443.	3.8	19

#	Article	IF	CITATIONS
73	Rationally designed hierarchical MnO2-shell/ZnO-nanowire/carbon-fabric for high-performance supercapacitor electrodes. Journal of Power Sources, 2014, 272, 654-660.	4.0	41
74	One-dimensional visible-light-driven bifunctional photocatalysts based on Bi4Ti3O12 nanofiber frameworks and Bi2XO6 (X=Mo, W) nanosheets. Applied Catalysis B: Environmental, 2014, 160-161, 757-766.	10.8	103
75	Hierarchical assembly of BiOCl nanosheets onto bicrystalline TiO2 nanofiber: Enhanced photocatalytic activity based on photoinduced interfacial charge transfer. Journal of Colloid and Interface Science, 2014, 435, 26-33.	5.0	40
76	<i>p</i> -MoO ₃ Nanostructures/ <i>n</i> -TiO ₂ Nanofiber Heterojunctions: Controlled Fabrication and Enhanced Photocatalytic Properties. ACS Applied Materials & Interfaces, 2014, 6, 9004-9012.	4.0	148
77	CuO/Cu ₂ O nanofibers as electrode materials for non-enzymatic glucose sensors with improved sensitivity. RSC Advances, 2014, 4, 31056.	1.7	79
78	BiOCl nanosheets immobilized on electrospun polyacrylonitrile nanofibers with high photocatalytic activity and reusable property. Applied Surface Science, 2013, 285, 509-516.	3.1	70
79	An electron-rich free-standing carbon@Au core–shell nanofiber network as a highly active and recyclable catalyst for the reduction of 4-nitrophenol. Physical Chemistry Chemical Physics, 2013, 15, 10453.	1.3	69
80	Hierarchical assembly of ultrathin hexagonal SnS ₂ nanosheets onto electrospun TiO ₂ nanofibers: enhanced photocatalytic activity based on photoinduced interfacial charge transfer. Nanoscale, 2013, 5, 606-618.	2.8	344
81	One-dimensional hierarchical heterostructures of In2S3 nanosheets on electrospun TiO2 nanofibers with enhanced visible photocatalytic activity. Journal of Hazardous Materials, 2013, 260, 892-900.	6.5	103
82	TiO2 nanoparticles immobilized on polyacrylonitrile nanofibers mats: a flexible and recyclable photocatalyst for phenol degradation. RSC Advances, 2013, 3, 7503.	1.7	44
83	In ₂ O ₃ nanocubes/carbon nanofibers heterostructures with high visible light photocatalytic activity. Journal of Materials Chemistry, 2012, 22, 1786-1793.	6.7	72
84	Hierarchical heterostructures of Bi2MoO6 on carbon nanofibers: controllable solvothermal fabrication and enhanced visible photocatalytic properties. Journal of Materials Chemistry, 2012, 22, 577-584.	6.7	196
85	Carbon-modified BiVO4 microtubes embedded with Ag nanoparticles have high photocatalytic activity under visible light. Nanoscale, 2012, 4, 7501.	2.8	82
86	Bi2MoO6 microtubes: Controlled fabrication by using electrospun polyacrylonitrile microfibers as template and their enhanced visible light photocatalytic activity. Journal of Hazardous Materials, 2012, 225-226, 155-163.	6.5	130
87	Controllable synthesis of Zn2TiO4@carbon core/shell nanofibers with high photocatalytic performance. Journal of Hazardous Materials, 2012, 229-230, 265-272.	6.5	26
88	Enhancement of the Visible-Light Photocatalytic Activity of In ₂ O ₃ –TiO ₂ Nanofiber Heteroarchitectures. ACS Applied Materials & Interfaces, 2012, 4, 424-430.	4.0	320
89	Tubular nanocomposite catalysts based on size-controlled and highly dispersed silver nanoparticles assembled on electrospun silicananotubes for catalytic reduction of 4-nitrophenol. Journal of Materials Chemistry, 2012, 22, 1387-1395.	6.7	251
90	In situ assembly of well-dispersed Au nanoparticles on TiO2/ZnO nanofibers: A three-way synergistic heterostructure with enhanced photocatalytic activity. Journal of Hazardous Materials, 2012, 237-238, 331-338.	6.5	113

#	Article	IF	CITATIONS
91	One-dimensional Bi2MoO6/TiO2 hierarchical heterostructures with enhanced photocatalytic activity. CrystEngComm, 2012, 14, 605-612.	1.3	228
92	Fabrication of Ag/TiO2 nanoheterostructures with visible light photocatalytic function via a solvothermal approach. CrystEngComm, 2012, 14, 3989.	1.3	225
93	In situ Generation of Well-Dispersed ZnO Quantum Dots on Electrospun Silica Nanotubes with High Photocatalytic Activity. ACS Applied Materials & Interfaces, 2012, 4, 785-790.	4.0	63
94	Bi2MoO6 ultrathin nanosheets on ZnTiO3 nanofibers: A 3D open hierarchical heterostructures synergistic system with enhanced visible-light-driven photocatalytic activity. Journal of Hazardous Materials, 2012, 217-218, 422-428.	6.5	86
95	Iron phthalocyanine/TiO2 nanofiber heterostructures with enhanced visible photocatalytic activity assisted with H2O2. Journal of Hazardous Materials, 2012, 219-220, 156-163.	6.5	67
96	In situ assembly of well-dispersed Ag nanoparticles (AgNPs) on electrospun carbon nanofibers (CNFs) for catalytic reduction of 4-nitrophenol. Nanoscale, 2011, 3, 3357.	2.8	566
97	Solvothermal synthesis and electrochemical properties of 3D flower-like iron phthalocyanine hierarchical nanostructure. Nanoscale, 2011, 3, 5126.	2.8	30
98	Bi4Ti3O12 nanosheets/TiO2 submicron fibers heterostructures: in situ fabrication and high visible light photocatalytic activity. Journal of Materials Chemistry, 2011, 21, 6922.	6.7	113
99	Core/shell nanofibers of TiO2@carbon embedded by Ag nanoparticles with enhanced visible photocatalytic activity. Journal of Materials Chemistry, 2011, 21, 17746.	6.7	143
100	In situ assembly of well-dispersed gold nanoparticles on electrospun silica nanotubes for catalytic reduction of 4-nitrophenol. Chemical Communications, 2011, 47, 3906.	2.2	276
101	Highly Efficient Decomposition of Organic Dye by Aqueous-Solid Phase Transfer and In Situ Photocatalysis Using Hierarchical Copper Phthalocyanine Hollow Spheres. ACS Applied Materials & Interfaces, 2011, 3, 2573-2578.	4.0	78
102	High Photocatalytic Activity of ZnOâ^'Carbon Nanofiber Heteroarchitectures. ACS Applied Materials & Interfaces, 2011, 3, 590-596.	4.0	415
103	TiO2@carbon core/shell nanofibers: Controllable preparation and enhanced visible photocatalytic properties. Nanoscale, 2011, 3, 2943.	2.8	187
104	Highly dispersed Fe3O4 nanosheets on one-dimensional carbon nanofibers: Synthesis, formation mechanism, and electrochemical performance as supercapacitor electrode materials. Nanoscale, 2011, 3, 5034.	2.8	299
105	Hierarchical Nanostructures of Copper(II) Phthalocyanine on Electrospun TiO ₂ Nanofibers: Controllable Solvothermal-Fabrication and Enhanced Visible Photocatalytic Properties. ACS Applied Materials & Interfaces, 2011, 3, 369-377.	4.0	194
106	Dandelion-like Fe3O4@CuTNPc hierarchical nanostructures as a magnetically separable visible-light photocatalyst. Journal of Materials Chemistry, 2011, 21, 12083.	6.7	54
107	Controllable fabrication of cadmium phthalocyanine nanostructures immobilized on electrospun polyacrylonitrile nanofibers with high photocatalytic properties under visible light. Catalysis Communications, 2011, 12, 880-885.	1.6	42
108	Tin oxide (SnO2) nanoparticles/electrospun carbon nanofibers (CNFs) heterostructures: Controlled fabrication and high capacitive behavior. Journal of Colloid and Interface Science, 2011, 356, 706-712.	5.0	88

#	Article	IF	CITATIONS
109	Zinc phthalocyanine hierarchical nanostructure with hollow interior space: Solvent–thermal synthesis and high visible photocatalytic property. Journal of Colloid and Interface Science, 2010, 348, 37-42.	5.0	45
110	Electrospun Nanofibers of <i>p</i> -Type NiO/ <i>n</i> -Type ZnO Heterojunctions with Enhanced Photocatalytic Activity. ACS Applied Materials & Interfaces, 2010, 2, 2915-2923.	4.0	574